Novel probe of charge symmetry breaking: Deuteron-induced deuteron breakup

C. R. Howell, P. D. Felsher,* W. Tornow, M. L. Roberts,† J. M. Hanly,‡ G. J. Weisel, M. Al Ohali, and R. L. Walter
Duke University and Triangle Universities Nuclear Laboratory, Durham, North Carolina 27708-0308

I. Šlaus
Rudjer Boškovic Institute, Zagreb, Croatia and Triangle Universities Nuclear Laboratory, Durham, North Carolina 27708-0308

J. M. Lambert and P. A. Treado§
Department of Physics, Georgetown University, Washington, D.C. 20057

G. Mertens
University of Tübingen, Tübingen, Germany
(Received 15 March 1993)

The present paper identifies unique symmetry properties of the $\vec{d} + d \rightarrow d + p + n$ breakup reaction that make it an excellent probe for studying charge-symmetry breaking. Measurements were made for two configurations of the ejected particles in the breakup reaction to obtain values of the spin observables A_y, A_{yy}, and A_{zz}. These observables are compared for the mirror reactions $^2\mathrm{H}(\vec{d}, dp)n$ and $^2\mathrm{H}(\vec{d}, dn)p$ for the two angle pairs $(\theta_d, \phi_d, \theta_N, \phi_N) = (17.0°, 0°, 17.0°, 180°)$ and $(17.0°, 0°, 34.5°, 180°)$ for an incident deuteron energy of 12 MeV. In addition, spin observables for the $^2\mathrm{H}(\vec{d}, pn)d$ reaction at $\theta_p = \theta_n$ and $\phi_p = \phi_n + 180°$ are shown to provide a particularly good test of charge symmetry. Our A_y, A_{yy}, and A_{zz} data for the $^2\mathrm{H}(\vec{d}, pn)d$ reaction at $(\theta_p, \phi_p, \theta_n, \phi_n) = (17.0°, 0°, 17.0°, 180°)$ are used to illustrate this latter point. Of the ten charge-symmetric sets of observables measured, two were found to differ by 2.5 standard deviations.

PACS number(s): 24.80.Dc, 24.70.+s, 25.45.−z, 21.45.+v

I. INTRODUCTION

The amount and quality of data accumulated over the last 25 years for the purpose of studying charge symmetry breaking (CSB) are impressive. However, it was not until recently that full understanding of the fundamental causes of the breaking of this symmetry in terms of quantum chromodynamics and the meson-exchange model of the nucleon-nucleon *(N-N)* force was achieved [1]. A remarkably consistent result is that about 90% of the observed CSB can be accounted for as being caused by ρ^0-ω mixing and the kinematic shift due to the mass differences between the neutron *(n)* and proton *(p)*, both of which are a reflection of the underlying mass difference between the up and down quarks [1]. For instance, the difference between the $^1S_0$ neutron-neutron *(n-n)* and proton-proton *(p-p)* scattering lengths (a_{nn} and a_{pp}, respectively), after correcting for electromagnetic (em) effects, can be fully accounted for by ρ^0-ω mixing in the *N-N* interaction [2,3]. The ^{3}H-^{3}He binding energy difference is now fully accounted for using em effects and the CSB forces due to ρ^0-ω mixing and the neutron-proton mass difference [4–6]. Even the binding energy differences between mirror nuclei, beyond that caused by em forces and first recognized by Nolen and Schiffer [7], can be shown to be mainly due to the CSB ρ^0-ω mixing in the *N-N* force [8]. With regard to recent *n-p* elastic scattering measurements at incident neutron energies of 183 MeV [9] and 477 MeV [10], the observed difference in the charge symmetric analyzing powers $\Delta A = A_{\vec{n}p} - A_{n\vec{p}}$ have been shown [9,10] at 183 MeV to be mainly caused by ρ^0-ω mixing in the *N-N* force [9] and at 477 MeV to be mainly a consequence of the *n-p* mass difference [11].

Though measurements of *n-p* elastic scattering with polarized neutron beams and polarized proton targets [9,10] provide information on isospin mixing between ^1P and ^3P waves and though the Nolen-Schiffer anomaly constrains the CSB in ^3P waves, our present knowledge of CSB in $l > 0$ waves is not adequate to construct a charge-dependent potential for the *N-NP* waves. Recent rigorous Faddeev-type calculations for the $A = 3$ system [12,13] and microscopic calculations for the $A = 4$ system [14,15] make it possible to reliably relate three-nucleon $(3N)$ and four-nucleon $(4N)$ scattering observables to details of the *N-N* force. These new calculations have shown that the vector analyzing powers in $A = 3$ and $A = 4$ scattering systems are strongly dependent on details of the ^3P-wave part of the *N-N* force [15,16]. It

*Present address: EG&G Rocky Flats, Golden, CO 80402-0464.
†Present address: Lawrence Livermore National Laboratory, Livermore, CA 94550.
‡Present address: Booz, Allen and Hamilton, Huntsville, AL 35806.
§Deceased.

is this dependence that makes these few-nucleon systems attractive for studying CSB in the *N-N P* waves ($l = 1$).

In the $A = 3$ system, differences between vector analyzing power (A_y) data for neutron-deuteron *(n-d)* and proton-deuteron *(p-d)* elastic scattering at low energies provide a measure of CSB. The main difficulty in interpreting these differences is discerning between differences that are due to CSB and those that are due to em forces (mostly the Coulomb force), since exact Faddeev calculations do not exist for *p-d* elastic scattering above the deuteron breakup threshold [17,18]. It has been shown using phenomenological calculations that the Coulomb repulsion of the incident proton in *p-d* scattering reduces the effective c.m. energy [19]. At present, the major concern with using *n-d* and *p-d* comparisons is that CSB effects can be masked by this Coulomb energy shift in *p-d* scattering [19].

In the $A = 4$ system, attempts have been made to observe CSB by comparing data for the $^2\mathrm{H}(\vec{d}, p)^3\mathrm{H}$ and $^2\mathrm{H}(\vec{d}, n)^3\mathrm{He}$ stripping reactions [20]. Although the Coulomb force in the entrance channel is identical, there are serious difficulties in using these reactions to obtain information on CSB. First, the Q values for the two reactions are different, and second, the Coulomb force in the exit channel is different in the two reactions.

Even though the $4N$ system is inherently more complicated than the $3N$ system and rigorous calculations using realistic *N-N* and Coulomb forces do not exist, we argue that the $d + d \rightarrow d + p + n$ breakup reaction is a more convenient probe to study CSB than other reactions involving more than two nucleons for the following reasons.

(1) Since the entrance channels are identical, ambiguity caused by the Coulomb energy shift in the entrance channel as in the case of *p-d* elastic scattering is avoided.

(2) Unlike the A_y data sets used in the *n-d* and *p-d* comparisons, the $^2\mathrm{H}(\vec{d}, dp)n$ and $^2\mathrm{H}(\vec{d}, dn)p$ data can be measured simultaneously, thereby canceling most instrumental asymmetries and the uncertainty in the incident beam polarization.

(3) With only minor technical difficulties, the use of tensor-polarized deuteron beams enables measurements of several charge-symmetric (CS) spin observables, whereas, in the case of nucleon-deuteron *(N-d)* elastic scattering a yet unavailable tensor-polarized deuterium target is required to make *n-d* tensor analyzing power measurements.

(4) Studying CS channels from the same breakup reaction avoids the Q-value complication that is inherent in the comparisons of data from the $^2\mathrm{H}(\vec{d}, p)^3\mathrm{H}$ and $^2\mathrm{H}(\vec{d}, n)^3\mathrm{He}$ reactions.

(5) Since the Coulomb force in momentum space is only dependent on the relative momentum and the charges of the interacting particles, the kinematic flexibility of the $d+d \rightarrow d+p+n$ reaction gives experimenters the capability of investigating Coulomb effects in the exit channels of the CS processes by varying the relative momentum of the emitted charged particles.

The above features of the $\vec{d} + d \rightarrow d + p + n$ breakup reaction might make it possible to deconvolute the Coulomb-force effects from those due to CSB. As stated above, since the relative momenta between the ejectiles can be varied independently of the c.m. energy, an empirical investigation of the Coulomb-force effects can be made. Once the influences of the Coulomb force are understood, one can then with confidence identify effects due to CSB. Of course, in order to relate such an observed CSB effect to the underlying *N-N* interaction, a rigorous $4N$ calculation is necessary.

In this paper we investigate the use of spin observables from the $\vec{d} + d \rightarrow d + p + n$ breakup reaction as a probe of CSB. The study is divided into two parts. In the first part, vector and tensor analyzing powers for the $^2\mathrm{H}(\vec{d}, dp)n$ and $^2\mathrm{H}(\vec{d}, dn)p$ CS channels are compared at identical kinematic conditions. The second part is a comparison of analyzing powers for the $^2\mathrm{H}(\vec{d}, pn)d$ reaction across symmetric halves of the kinematically allowed locus. The measurements in both parts are made in the kinematic region around the quasifree scattering (QFS) condition, deuteron-nucleon *(d-N)* QFS in the first part and *N-N* QFS in the second part. We had little to guide the precision needed in our measurements to observe differences between CS observables, since rigorous $4N$ calculations for this reaction are not available and prior to the data collected in the present work no data for CS spin observables for the $d + d \rightarrow d + p + n$ breakup reaction existed for incident deuteron energies below 50 MeV. The main goal of this study is to compare data for CS spin observables for the $d + d \rightarrow d + p + n$ breakup reaction at several reaction angles.

II. EXPERIMENTAL DETAILS

We have measured vector analyzing powers A_y and tensor analyzing powers A_{yy}, and A_{zz} for $^2\mathrm{H}(\vec{d}, dp)n$, $^2\mathrm{H}(\vec{d}, dn)p$, and $^2\mathrm{H}(\vec{d}, pn)d$ reactions at an incident deuteron energy of 12 MeV. Two of the three outgoing particles from the $\vec{d}+d \rightarrow d+p+n$ breakup reaction were detected in coincidence on opposite sides of the incident beam axis. The angle pairs were chosen to select the kinematic region for *d-N* QFS. All measurements were conducted at the Triangle Universities Nuclear Laboratory (TUNL).

A. Experimental setup

A diagram of the experimental setup is shown in Fig. 1. The target was a 2.5-cm-diam cylindrical gas cell filled with 1.0 bar of deuterium. The gas was contained by an 8-μm-thick uncoated Kapton foil. The incident beam energy was adjusted so that the energy at the center of the deuterium target was 12 MeV. The beam was collimated by two sets of slits just before the entrance to the scattering chamber to produce a square beam spot on target of area 1 mm^2. The beam current was measured on a suppressed beam stop 2 m downstream of the scattering chamber. The beam stop was shielded using lithium-loaded paraffin to reduce the background in the

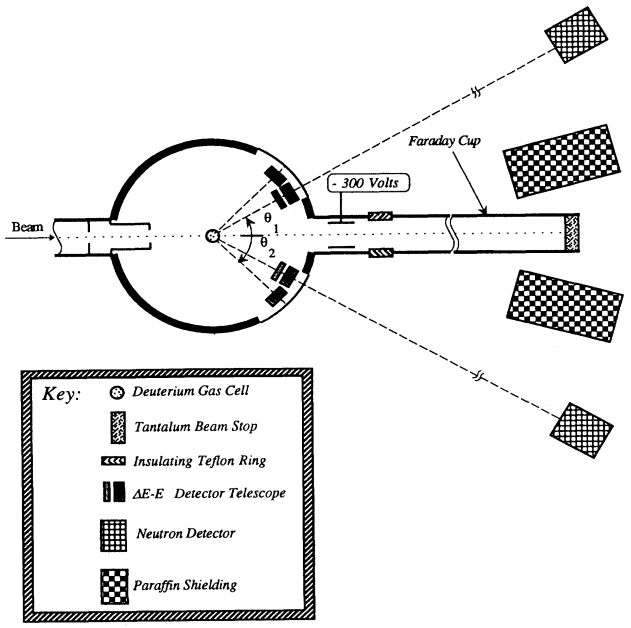

FIG. 1. Top view of experimental setup for $\vec{d}+d \rightarrow d+p+n$ breakup measurements.

neutron detectors. Emitted charged particles were detected by silicon surface barrier detectors located inside an evacuated scattering chamber as shown in Fig. 1. The angular range subtended by each charged-particle detector was defined by a set of rectangular slits. The intensity of the incident dc polarized beam was kept below about 25 nA on target as a compromise between the coincidence counting rate and pileup in the charged-particle energy spectrum. Also, since uncoated Kapton is not a good heat conductor, the low beam current reduced the chance of rupturing the gas cell.

Neutrons were detected with two rectangular 7.62 wide $\times$ 15.24 high $\times$ 10.16 thick cm^3 liquid scintillators, which enabled the use of pulse-shape discrimination against γ rays. The neutron detectors were positioned 2.65 m from the center of the deuterium target. To reduce attenuation of neutrons passing through the 1-cm-thick aluminum wall of the scattering chamber, an opening was cut in the chamber wall on both sides of the incident beam axis as shown in Fig. 1. Each opening spanned the angular region between 16° and 40° and was covered with a 0.64-mm-thick stainless steel plate to maintain the chamber vacuum. The center of all detectors were located in the horizontal scattering plane. To reduce the effects of instrumental asymmetries, detectors were positioned symmetrically about the axis defined by the incident deuteron beam, as shown in Fig. 1, and the direction of the spin quantization axis was reversed every 15 min at the source.

B. Detector geometry and experimental energy resolution

The description of our right-handed coordinate system is as follows. The $+z$ axis is in the direction of the incident beam. The horizontal plane contains the x and z axes with the $+x$ axis pointing to the left as seen along the direction of the incident beam. The $+y$ axis is given by $\hat{z}\times\hat{x}$. The polar angle θ is measured from the $+z$ axis, and the azimuthal angle ϕ is measured up from the $+x$ axis to the half-plane containing the detector and the $+z$ axis. In a kinematically complete three-body (3B) breakup reaction five kinematic variables uniquely define the point in phase space at which the observable is measured. In our measurements of the $\vec{d}+d \rightarrow d+p+n$ reaction, we determine the angles and energies of two of the emitted particles $(\theta_1, \phi_1, \theta_2, \phi_2, E_1, E_2)$, thus kinematically overdetermining the reaction. Since in the present measurements the detectors were always located in the x-z plane, the shorthand notation (θ_1, θ_2) will be used to represent $(\theta_1, \phi_1, \theta_2, \phi_2)$ for the angles of the detected particles with the sign convention $\theta > 0°$ for $\phi = 0°$ and $\theta < 0°$ for $\phi = 180°$. For example, in the case of the deuteron-neutron *(d-n)* coincidence measurements, we specify the tensor analyzing powers as $A_{ii}(\theta_d, \theta_n, E_d, E_n)$, where i represents either x, y, or z.

The data were accumulated in three measurements: (I) $(\theta_d, \theta_p) = (+17.0°, -17.0°)$, $(\theta_d, \theta_n) = (+17.0°, -17.0°)$, and $(\theta_p, \theta_n) = (+17.0°, -17.0°)$; (II) $(\theta_d, \theta_p) = (+17.0°, -17.0°)$ and $(\theta_d, \theta_n) = (+17.0°, -34.5°)$; and (III) $(\theta_d, \theta_p) = (+17.0°, -17.0°)$ and $(\theta_d, \theta_p) =$

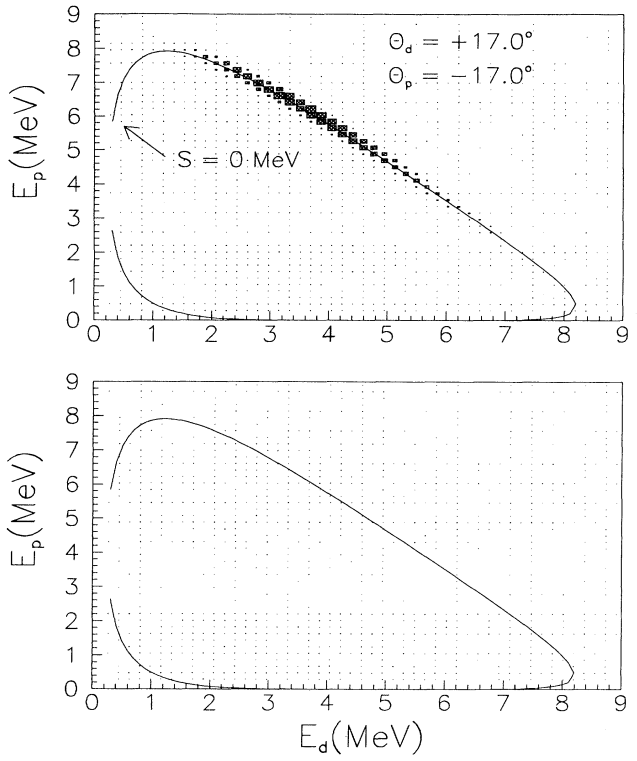

FIG. 2. Two-dimensional histogram of the detected deuteron energy E_d at $\theta = +17.0°$ vs the energy E_p of the detected proton at $\theta = -17.0°$. The top spectrum contains both "true" and "accidental" coincidence counts, while the bottom spectrum contains only "accidental" counts. The curve is the kinematically allowed locus of E_d vs E_p.

$(+17.0°, -34.5°)$. Each detector pair was mirrored about the beam axis. The $(\theta_d, \theta_p) = (+17.0°, -17.0°)$ angle pair provided a consistency check between the three measurements. The charged-particle detectors at 17.0° were ΔE-E telescopes and thereby provided particle identification. Since only E detectors were used for charged-particle detection at 34.5° in the third measurement, particle identification was not possible at this angle. In the first two measurements, the angle subtended by the ΔE-E telescope located at 17.0° was $(\Delta\theta = \pm 1.8°, \Delta\phi = \pm 1.27°)$. The angular spread of the neutron detector was $(\Delta\theta = \pm 0.90°, \Delta\phi = \pm 1.65°)$. In the third measurement the angular spreads in the 17.0° and 34.5° detectors were $(\Delta\theta = \pm 2.0°, \Delta\phi = \pm 0.90°)$ and $(\Delta\theta = \pm 1.8°, \Delta\phi = \pm 1.08°)$, respectively. The data from the three measurements were combined statistically to give three sets of CS data: $(\theta_d, \theta_N) = (+17.0°, -17.0°)$, $(\theta_d, \theta_N) = (+17.0°, -34.5°)$, and $(\theta_p, \theta_n) = (+17.0°, -17.0°)$.

A coincidence event was defined as one in which there was an event in one of the 17° detectors and an event in a detector on the opposite side of the beam axis within 50 ns for deuteron-proton *(d-p)* coincidences and within 180 ns for *d-n* and proton-neutron *(p-n)* coincidences. Accidental coincidences were measured simultaneously with the primary data using a second coincidence circuit in which the signals from one of the detectors in the pair were delayed by 300 ns. For the *d-p* coincidences the data were sorted into two-dimensional (2D) histograms of deuteron energy (E_d) versus proton energy (E_p) as shown in Fig. 2. The top spectrum contains both "true" and "accidental" events, whereas the bottom spectrum contains only "accidentals." The grey scaling is the same for the top and bottom spectra. The curve in Fig. 2, commonly referred to as the S curve, is the calculated locus of E_d versus E_p. The experimental data are smeared around the calculated locus due to experimental energy and angle resolution. The angle resolution has been discussed above and the experimental energy resolution is summarized in Table I.

C. Projection of data onto the S curve

The data points were projected onto the S curve using a minimum distance technique similar to that of Zeitnitz *et al.* [21]. All data points lying within 250 keV of the S curve were projected. The projected data were summed into 250-keV bins along S. A projected spectrum is shown in Fig. 3 for the *d-p* coincidence at $(\theta_d, \theta_p) = (+17.0°, -17.0°)$. The projection of the accidental events is represented by the dashed curve. The coincidence data involving neutrons were projected using the same technique; however, because of the poorer energy resolution of the time-of-flight (TOF) technique for determining the neutron energy (documented in Table I), all data within 500 keV of the S curve were projected. Spectra of the projected "true+accidental" (solid curve) and "accidental" (dashed curve) data for the *d-n* coincidence at $(\theta_d, \theta_n) = (+17.0°, -17.0°)$ are shown in Fig. 4. The accidentals are slightly higher in the *d-n* coincidence spectrum than in the corresponding *d-p* spectrum because of the room background in the neutron detector and the wider timing on the *d-n* coincidence window.

The experimental energy resolution along the S curve is given by

$$\Delta S(E_1, E_2) = \left[\left(\frac{\delta S}{\delta E_1} \right)^2 \Delta {E_1}^2 + \left(\frac{\delta S}{\delta E_2} \right)^2 \Delta {E_2}^2 \right]^{\frac{1}{2}}, \quad (1)$$

where ΔE_1 and ΔE_2 are the energy spreads for the particles detected at the angles θ_1 and θ_2, respectively. Because the energy of the detected neutrons was determined from the TOF difference between the neutron and the associated charged particle, the neutron TOF had to be corrected for the flight time of the charged particle. The neutron energy resolution shown in Table I includes the uncertainty of the charged-particle flight time. Since ΔE_1 and ΔE_2 are functions of E_1 and E_2, the value of ΔS varies along the S curve. For instance, for the

TABLE I. Experimental energy resolution. Because the energy resolution is dependent on the energy of the detected particles, it has been computed at two extreme energies, 8 and 3 MeV. The values in parentheses are for 3-MeV particles. All values are full width at half maximum.

Effect		Detected particle neutron ΔE keV	proton ΔE	deuteron ΔE
Detector resolution		393 (90)[a]	20	20
Straggle in Kapton foil	(incident)	6	6	6
	(exit)		5 (10)	8 (17)
Target thickness[b]	(incident)	14	14	14
	(exit)	617 (231)[c]	20 (46)	36 (82)
Total		732 (248)	33 (53)	45 (87)

[a]These values include the intrinsic time resolution of the detector (Δt = 1.5 ns) and the time dispersion of the associated charged particle due to the finite extent of the target (Δt = 0.71 ns for a 3-MeV outgoing deuteron).

[b]The average thickness of the target viewed by all detectors is 2 cm.

[c]Dispersion in neutron energy measurement due to flight path difference caused by finite extent of the deuterium gas target and thickness of neutron detector.

d-n coincidence at $(\theta_d, \theta_n) = (+17.0°, -17.0°)$, the energy spread in S at 3 MeV prior to the QFS point ($S = 2.25$ MeV), at the QFS point ($S = 5.25$ MeV), and 3 MeV after the QFS point ($S = 8.25$ MeV) is 233, 388, and 221 keV, respectively. Because the energy spread in the d-n coincidence data was often greater than the 250-keV energy bins along the S curve, both the d-n and d-p coincidence data were integrated over a ΔS of 750 keV by summing together three of the 250-keV bins. This assured that the d-n and d-p coincidence data were compared over the same energy intervals along the S curve.

D. Determination of analyzing powers from projected spectra

The net yields, "true + accidental" minus "accidentals," in each bin of the projected spectra were used to compute the analyzing powers A_y, A_{yy}, and A_{zz}. The yields for a particular (θ_1, θ_2, S) value for the $\vec{d} + d \rightarrow d + p + n$ breakup reaction using a polarized incident deuteron beam can be written for a coplanar geometry as [22]

$$N(\theta_1,\theta_2,S) = N_0(\theta_1,\theta_2,S)\left\{1 + \frac{3}{2}P_z A_y(\theta_1,\theta_2,S)\sin\beta\cos\gamma - P_{zz}A_{xz}(\theta_1,\theta_2,S)\sin\beta\cos\beta\sin\gamma \right.$$
$$-\frac{1}{4}P_{zz}\left[A_{xx}(\theta_1,\theta_2,S) - A_{yy}(\theta_1,\theta_2,S)\right]\sin^2\beta\cos 2\gamma$$
$$\left.+\frac{1}{4}P_{zz}A_{zz}(\theta_1,\theta_2,S)\left[3\cos^2\beta - 1\right]\right\}. \quad (2)$$

In the above equation $N_0(\theta_1, \theta_2, S)$ is the yield obtained using an unpolarized beam; the parameters [23] P_z and P_{zz} are the vector and tensor beam polarization moments, respectively; A_y, A_{xz}, A_{xx}, A_{yy}, and A_{zz} are the Cartesian vector and tensor analyzing powers as functions of θ_1, θ_2, and S; the angles β and γ define the orientation of the spin quantization axis $\hat{\mathbf{s}}$ of the incident beam [23]; the angles θ_1 and θ_2 are the laboratory angles of the two detected particles; and S is the centroid of the energy bin along the kinematic locus.

All measurements were made using a four-step sequence consisting of two values of the beam polarization moments with a reversal of the direction of $\hat{\mathbf{s}}$ for each moment setting. For the first two steps, the values of the magnetic fields in the spin filter and charge-exchange canal on the Lamb-shift polarized ion source at TUNL [24] were set to deliver a beam with $P_z = P_{zz} = +1$. The magnetic field strengths were changed for the second two steps to deliver $P_z = 0$ and $P_{zz} = -2$. The actual beam polarization was about 70% of these theoretical values. The $\hat{\mathbf{s}}$ vector was flipped by reversing the direction of the axial magnetic fields in the source. By mirroring the detectors about the incident beam axis and flipping the spin quantization axis, most instrumental asymmetries [25] were canceled. Data were accumulated for 15 min in each step and the four-step sequence was repeated until the desired statistical accuracy was obtained.

The unit normal to the scattering plane is determined in the usual way:

$$\hat{\mathbf{n}} = \left(\hat{\mathbf{k}}_{\text{in}} \times \hat{\mathbf{k}}_{\text{out}}\right) \Big/ \left|\hat{\mathbf{k}}_{\text{in}} \times \hat{\mathbf{k}}_{\text{out}}\right|, \quad (3)$$

where $\hat{\mathbf{k}}_{\text{in}}$ is the direction of the incident beam momentum ($\hat{\mathbf{z}}$) and $\hat{\mathbf{k}}_{\text{out}}$ is the direction of the outgoing deuteron

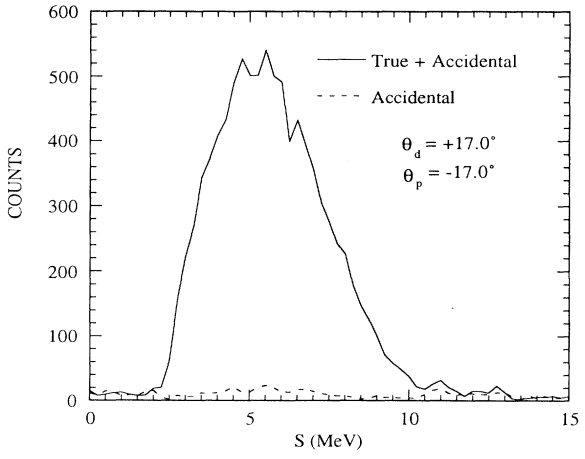

FIG. 3. Spectra of data for the d-p coincidence at $(\theta_d, \theta_p) = (+17.0°, -17.0°)$ projected onto the kinematic S curve. The solid and dashed curves represent the "true + accidental" and "accidental" data, respectively.

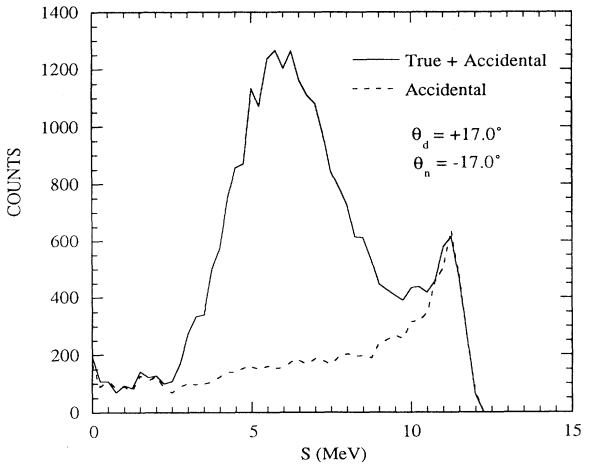

FIG. 4. Same as Fig. 3 except for the d-n coincidence $(\theta_d, \theta_n) = (+17.0°, -17.0°)$.

in the *d-N* coincidences and the direction of the emitted proton in the case of the *p-n* coincidences. The angles β and γ in Eq. (2) are defined as [22]

$$\cos\beta = \hat{\mathbf{s}} \cdot \hat{\mathbf{k}}_{\text{in}} \tag{4}$$

and

$$\cos\gamma = \hat{\mathbf{s}} \cdot \hat{\mathbf{n}} / \sin\beta. \tag{5}$$

So for *d-N (p-n)* coincidences with $\hat{\mathbf{s}} = \hat{\mathbf{y}}$ and the detected deuteron (proton) on the left side $\theta_d > 0°$ ($\theta_p > 0°$) and $\gamma = 0°$, the mirrored arrangement has the deuteron (proton) detected on the right side $\theta_d < 0°$ ($\theta_p < 0°$) and $\gamma = 180°$. For convenience we shall refer to these as left-side and right-side coincidences. The analyzing powers were computed from the geometrical mean of the yields from the left- and right-side coincidences for the four data acquisition steps. The mean yields were computed as

$$N_{1\uparrow} = \sqrt{L_{1\uparrow}R_{1\downarrow}},\ N_{1\downarrow} = \sqrt{L_{1\downarrow}R_{1\uparrow}},$$
$$N_{2\uparrow} = \sqrt{L_{2\uparrow}R_{2\downarrow}},\ N_{2\downarrow} = \sqrt{L_{2\downarrow}R_{2\uparrow}}. \tag{6}$$

Here L and R represent the left-side and right-side coincidence yields for identical kinematic conditions. The first subscript denotes the setting of the beam moments, with the number 1 corresponding to $P_z = P_{zz} = +1$, and the number 2 for the setting $P_z = 0$ and $P_{zz} = -2$. The arrow subscript represents the relative helicity of the spin quantization axis.

Because the A_{zz} measurements required a different orientation of $\hat{\mathbf{s}}$ than A_y and A_{yy}, it was determined separately. In the A_{zz} measurements, $\hat{\mathbf{s}}$ was parallel ($\beta = 0°$) or antiparallel ($\beta = 180°$) to the incident beam momentum. In this case the angle γ is undefined [see Eq. (5)]. For each data acquisition step an equation for the yields was obtained using Eq. (2). The four equations were solved for A_{zz} with

$$A_{zz} = \frac{2\Big[(N_{2\uparrow} + N_{2\downarrow}) - (N_{1\uparrow} + N_{1\downarrow})\Big]}{(N_{1\uparrow} + N_{1\downarrow})\,P_{zz}^{(2)} - (N_{2\uparrow} + N_{2\downarrow})\,P_{zz}^{(1)}}. \tag{7}$$

The $P_{zz}^{(1)}$ and $P_{zz}^{(2)}$ are the actual values of P_{zz} for the first two and second two steps of the data taking sequence, respectively.

The values for A_y and A_{yy} were determined simultaneously using the same procedure as described above. In this case, the angle β was fixed to 90° and γ was flipped between 0° and 180°. The resulting expressions for A_{yy} and A_y are

$$A_{yy} = \frac{2\Big[(N_{2\uparrow} + N_{2\downarrow}) - (N_{1\uparrow} + N_{1\downarrow})\Big]}{(N_{1\uparrow} + N_{1\downarrow})\,P_{zz}^{(2)} - (N_{2\uparrow} + N_{2\downarrow})\,P_{zz}^{(1)}} \tag{8}$$

and

$$A_y = \frac{N_{1\uparrow} - N_{1\downarrow}}{N_{2\uparrow} + N_{2\downarrow}} \left[\frac{2 + P_{zz}^{(2)} A_{yy}}{3P_z^{(1)}}\right], \tag{9}$$

where $P_z^{(1)}$ is the vector moment of the beam in steps 1 and 2.

III. RESULTS AND DISCUSSION

The presentation of the results has been divided into two parts: (1) the comparison of *d-p* and *d-n* coincidence data at identical kinematic conditions and (2) the comparison of *p-n* coincidence data at different points along the kinematically allowed S curve for the special case of $\theta_n = -\theta_p$. A summary of the results is given in Table II and discussed below.

A. Uncertainties

The uncertainties (combined statistical and systematic) in these data ranged from ±0.007 near the QFS peak to ±0.060 near the extremes of the kinematic locus. The main systematic error was due to the uncertainty in the incident deuteron beam polarization which was determined using the quench-ratio method [26]. For this work a conservative uncertainty of ±2% of the beam polarization was assigned ($\Delta P_z^{(1)} = \Delta P_{zz}^{(1)} = \pm 0.015$ and $\Delta P_z^{(2)} = 0$ and $\Delta P_{zz}^{(2)} = \pm 0.030$). The effect of this uncertainty on the errors in the analyzing powers can be derived using Eqs. (7)–(9). All data in the comparisons below are binned in 750-keV steps. This exceeds the experimental energy resolution (see Table I).

TABLE II. The A_y, A_{yy}, and A_{zz} data obtained in this work averaged over the arc from $S_a(E_1, E_2)$ to $S_b(E_1', E_2')$.

Detected particles	(θ_1, θ_2)	$S_a(E_1, E_2)$–$S_b(E_1', E_2')$ (MeV)	$A_y \pm \Delta A_y$	$A_{yy} \pm \Delta A_{yy}$	$A_{zz} \pm \Delta A_{zz}$
dn	(+17.0°, −17.0°)	3.9(2.5, 7.2)–9.9(6.6, 2.8)	0.024 ± 0.003	0.003 ± 0.004	0.040 ± 0.003
dp	(+17.0°, −17.0°)	3.9(2.5, 7.2)–9.9(6.6, 2.8)	0.018 ± 0.003	0.001 ± 0.004	0.037 ± 0.004
dn	(+17.0°, −34.5°)	4.6(3.8, 5.6)–9.9(7.6, 2.1)	0.021 ± 0.009	0.107 ± 0.012	−0.105 ± 0.017
dp	(+17.0°, −34.5°)	4.6(3.8, 5.6)–9.9(7.6, 2.1)	0.029 ± 0.014	0.100 ± 0.019	−0.165 ± 0.019
pn	(+17.0°, −17.0°)	3.9(2.5, 6.8)–6.4(4.4, 5.2)	0.011 ± 0.010	0.044 ± 0.013	−0.032 ± 0.013
pn	(+17.0°, −17.0°)	7.6(5.2, 4.3)–10.1(6.9, 2.4)	−0.016 ± 0.012	0.021 ± 0.016	−0.027 ± 0.016
pn	(+17.0°, −17.0°)	6.4(4.4, 5.2)–7.6(5.2, 4.3)	0.035 ± 0.013	0.038 ± 0.018	0.010 ± 0.017

B. Comparison of *d-p* and *d-n* coincidence data

We have measured the analyzing powers for the *d-p* and *d-n* coincidences at *d-N* angle pairs $(\theta_d, \theta_N) = (+17.0°, -17.0°)$ and $(+17.0°, -34.5°)$. Figure 5 shows the data for $(\theta_d, \theta_N) = (+17.0°, -17.0°)$ plotted as a function of arc length along the S curve. Much of the *d-p* and *d-n* coincidence data were accumulated simultaneously to reduce the influences of systematic errors in these comparisons. As stated before, the relative difference in the analyzing powers for the CS pairs is not influenced by the uncertainty in the incident beam polarization. Nevertheless, we combined this error with the statistical errors; the influence is nearly negligible. To reduce statistical uncertainties, the data were averaged over the region S = 3.9–9.9 MeV where the *d-p* and *d-n* coincidence measurements overlapped. As shown in Table II, the differences in A_y, A_{yy}, and A_{zz} for the two processes in the above interval are 0.006 ± 0.004, 0.002 ± 0.006, and 0.003 ± 0.005, respectively. We note that the data for the two reactions are indistinguishable within statistical uncertainties.

The data for $(\theta_d, \theta_N) = (+17.0°, -34.5°)$ are shown in Fig. 6. These data were averaged over the region S = 4.6–9.9 MeV where the *d-p* and *d-n* coincidence measurements overlap (see Table II). The A_y and A_{yy} data for the two processes agree within experimental uncertainties (see Table II). However, there is a significant difference of 0.060 ± 0.025 between the *d-p* and *d-n* A_{zz} data.

C. *p-n* coincidence data

In addition to studying the $^2\mathrm{H}(\vec{d}, dN)$ reactions, we made polarization measurements of the $^2\mathrm{H}(\vec{d}, pn)d$ reaction at $(\theta_p, \theta_n) = (+17.0°, -17.0°)$. If CS is valid, then the A_{yy} and A_{zz} along the kinematic locus in a plot of E_p vs E_n (of the type shown in Fig. 2 for E_d vs E_p) should be symmetric with respect to the $E_p = E_n$ point and A_y should be asymmetric with respect to the same point. This feature can be proven as follows. Since tensor analyzing powers for measurements made with the spin quantization axis of the beam oriented along a coordinate axis are invariant under a 180° rotation about the z axis [23], one can write

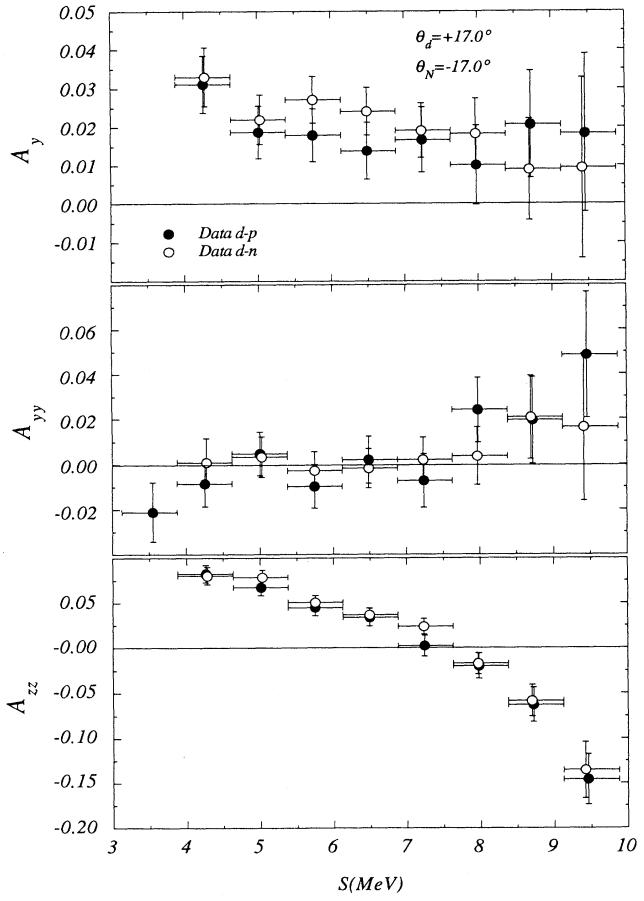

FIG. 5. Vector A_y and tensor A_{yy} and A_{zz} analyzing power data for the reactions $^2\mathrm{H}(\vec{d}, dp)n$ (solid circles) and $^2\mathrm{H}(\vec{d}, dn)p$ (open circles) as a function of the arc length S for $(\theta_d, \theta_N) = (+17.0°, -17.0°)$. The horizontal bars indicate the 750-keV interval along the arc which that point spans.

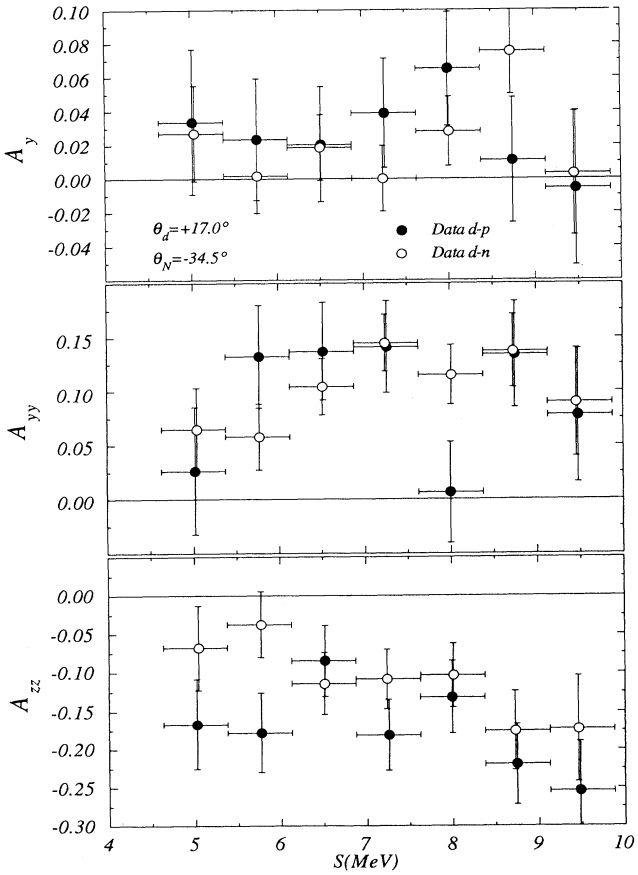

FIG. 6. Same as Fig. 5, except for $(\theta_d, \theta_N) = (+17.0°, -34.5°)$.

$$A_{ii}(\theta_p = +\theta, \theta_n = -\theta, E_p = E_1, E_n = E_2) = A_{ii}(\theta_p = -\theta, \theta_n = +\theta, E_p = E_1, E_n = E_2), \quad (10)$$

where the particle angles and energies are as specified in Sec. II. If charge symmetry holds, then

$$A_{ii}(\theta_p = -\theta, \theta_n = +\theta, E_p = E_1, E_n = E_2) = A_{ii}(\theta_p = +\theta, \theta_n = -\theta, E_p = E_2, E_n = E_1). \quad (11)$$

Therefore, we obtain the symmetric relationship

$$A_{ii}(\theta_p = +\theta, \theta_n = -\theta, E_p = E_1, E_n = E_2) = A_{ii}(\theta_p = +\theta, \theta_n = -\theta, E_p = E_2, E_n = E_1). \quad (12)$$

This simply means that if CS holds, the tensor analyzing powers such as A_{yy} and A_{zz} must be symmetric about the $E_p = E_n$ point along the locus of E_p vs E_n. And since A_y is antisymmetric under a 180° rotation about the z axis [23], the A_y for the breakup reaction must be antisymmetric about the $E_p = E_n$ point on the locus. Therefore, the value of A_y at the $E_p = E_n$ point must be equal to zero.

The A_y, A_{yy}, and A_{zz} data for the reaction $^2\mathrm{H}(\vec{d}, pn)d$ at $(\theta_p, \theta_n) = (+17.0°, -17.0°)$ are shown in Fig. 7 and are compared in Table II in two regions S = 3.9–6.4 and 7.6–10.1 MeV that are symmetric about the $E_p = E_n$ point at S = 7 MeV. The A_{yy} and A_{zz} data are symmetric to within the uncertainties of ±0.025 and the A_y data are antisymmetric to within their statistical uncertainties of ±0.016. However, in the 1.2-MeV-wide interval S = 6.4–7.6 MeV, which brackets the $E_p = E_n$ point (S = 7 MeV), the value of A_y is 0.035 ± 0.013, not zero, as it should be if CS holds. The width of this interval is roughly 3 times the experimental energy resolution (see Table I).

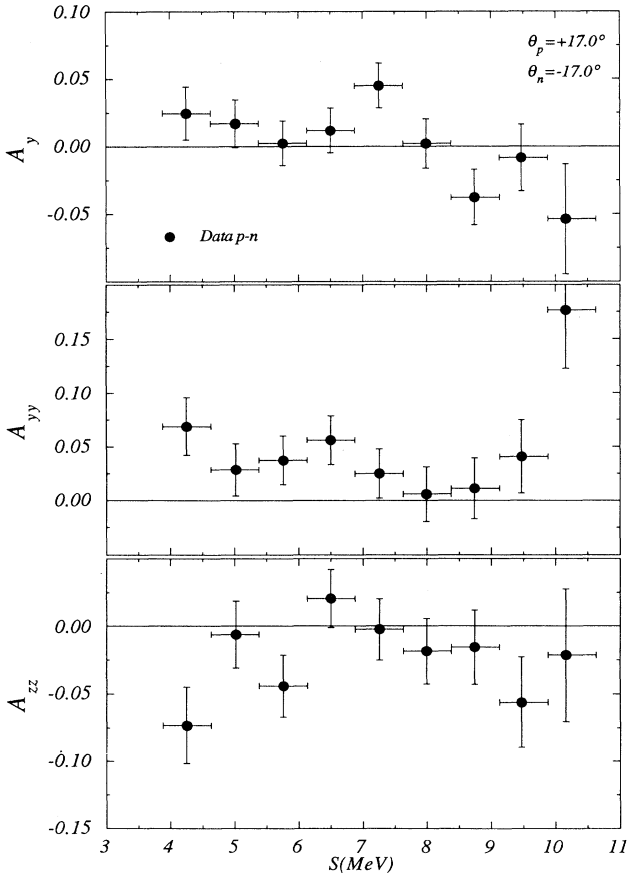

FIG. 7. Vector A_y and tensor A_{yy} and A_{zz} analyzing power data for the $^2\mathrm{H}(\vec{d}, pn)d$ reactions as a function of the arc length S for $(\theta_p, \theta_n) = (+17.0°, -17.0°)$. The horizontal bars indicate the 750-keV interval along the arc which that point spans.

IV. CONCLUSIONS

This paper points out the salient features of this novel probe of CSB, and describes experimental investigations using this probe. We have used the three sets of CS data measured in this work to investigate the influence of the Coulomb force on spin observables for the $\vec{d} + d \rightarrow d + p + n$ breakup reaction. By choosing the particle emission angles, the relative momenta of the two emitted charged particles (the deuteron and proton) in the two CS reactions can be varied. Since the magnitude of the relative momentum between the outgoing deuteron and proton is proportional to the relative energy E_{dp}, we refer to relative energies instead of relative momenta. For example, for the d-N angle pair $(+17.0°, -17.0°)$ in the energy interval S = 3.9–9.9 MeV, the average E_{dp} are 1.06 and 1.83 MeV for the $^2\mathrm{H}(\vec{d}, dn)p$ and $^2\mathrm{H}(\vec{d}, dp)n$ reactions, respectively. Because the A_y, A_{yy}, and A_{zz} data for the $^2H(\vec{d}, dn)p$ and $^2H(\vec{d}, dp)n$ reactions are identical within statistics, we conclude that Coulomb effects are unimportant in the comparison of CS spin observables for this range of E_{dp}. Either the Coulomb effects are negligible or they are identical for the two CS channels of the reaction. For the d-N angle pair $(+17.0°, -34.5°)$ the average E_{dp} over the interval S = 4.6–9.9 MeV are 2.20 and 1.66 MeV for the $^2\mathrm{H}(\vec{d}, dn)p$ and $^2\mathrm{H}(\vec{d}, dp)n$ reactions, respectively. For this angle pair, the A_y as well as the A_{yy} data for these two CS channels are identical within statistics. This is expected since the Coulomb effects should be smaller here than for $(\theta_d, \theta_N) = (+17.0°, -17.0°)$ where the values of E_{dp} are lower. For the p-n angle pair at $(+17.0°, -17.0°)$, the average E_{dp} in the first interval, S = 3.9–6.4 MeV, is 1.4 MeV and in the second interval, S = 7.6–10.1 MeV, is 3.0 MeV. The good agreement of the CS p-n coincidence data validates our above findings with the d-N data that Coulomb effects are negligible for E_{dp} values as low as 1.06 MeV.

Our measurements show that at these energies the spin observables for the $\vec{d} + d \rightarrow d + p + n$ breakup have relatively sizable magnitudes, i.e., up to 0.2. Also, the large cross section of about 10 mb/(sr^2 MeV) along the locus allowed us to perform measurements with an overall uncertainty below ± 0.001 for spin observables A_y, A_{yy}, and A_{zz} for a ΔS interval of 750 keV. This accuracy is illustrated by our data at $(\theta_d, \theta_N) = (+17.0°, -17.0°)$.

The results discussed above provide us with a qualitative understanding of the dependence of the CS observables on the Coulomb force. Of the ten CS observables in this work, eight are identical to within uncertainties of ± 0.003 to ± 0.02. Only the A_y data at $(\theta_p, \theta_n) = (+17.0°, -17.0°)$ and the A_{zz} data at $(\theta_d, \theta_N) = (+17.0°, -34.5°)$ indicated a breaking of charge symmetry, but even then only at the level of 2.5 standard deviations.

We realize that these two discrepancies cannot be interpreted as a clear signal for CSB; however, we note that six out of seven S bins in Fig. 6 show A_{zz} at $(\theta_d, \theta_N) = (+17.0°, -34.5°)$ for d-n to be less negative than for d-p, and that the A_y values at $(\theta_p, \theta_n) = (+17.0°, -17.0°)$ centered around $S = 7$ MeV are positive by two to three standard deviations from zero irrespective of the choice of the S intervals.

The results of this study demonstrate the power of the $\vec{d} + d \rightarrow d + p + n$ breakup reaction as a probe of CSB. It is clearly important to investigate this reaction more thoroughly and to perform measurements to an accuracy of better than ± 0.01 for 750 keV energy intervals, which is the accuracy of our $(\theta_p, \theta_n) = (+17.0°, -17.0°)$ data. In addition, it is important to disentangle the influences of the Coulomb force and CSB effects. Perhaps this could be accomplished by performing measurements at a greater variety of ejectile angle pairs and at several incident deuteron energies.

This work was supported in part by the U.S. Department of Energy, Office of High Energy and Nuclear Physics, under Grant No. DEFG05-91-ER40619, the U.S.-former Yugoslavia Joint Board under Contract No. JF682, and the Deutsche Forschungsgemeinschaft under Contract No. Me544/8-1.

[1] G. A. Miller, B. M. K. Nefkens, and I. Šlaus, Phys. Rep. **194**, 1 (1990).
[2] I. Šlaus, Y. Akaishi, and H. Tanaka, Phys. Rep. **173**, 257 (1989).
[3] S. A. Coon and R. C. Barrett, Phys. Rev. C **36**, 2189 (1987).
[4] Y. Wu, S. Ishikawa, and T. Sasakawa, Phys. Rev. Lett. **64**, 1875 (1990).
[5] J. L. Friar, B. F. Gibson, and R. L. Payne, Phys. Rev. C **35**, 1502 (1987).
[6] R. A. Brandenburg *et al.*, Phys. Rev. C **37**, 781 (1988).
[7] J. S. Nolen, Jr. and J. P. Schiffer, Annu. Rev. Nucl. Phys. **19**, 471 (1969).
[8] P. G. Blunden and M. J. Iqbal, Phys. Lett. B **198**, 14 (1987).
[9] L. D. Knutson *et al.*, Phys. Rev. Lett. **66**, 1410 (1991).
[10] R. Abegg *et al.*, Phys. Rev. Lett. **56**, 2571 (1986).
[11] G. A. Miller, A. W. Thomas, and A. G. Williams, Phys. Rev. Lett. **56**, 2567 (1986); Phys. Rev. C **36**, 1956 (1987).
[12] H. Witala, T. Cornelius, and W. Glöckle, Few-Body Syst. **3**, 123 (1988); H. Witala, W. Glöckle, and T. Cornelius, Few-Body Syst. Suppl. **2**, 555 (1987).
[13] C. R. Howell *et al.*, Phys. Rev. Lett. **61**, 1565 (1988).
[14] T. E. Mdlalose, H. Fiedelday, and W. Sandhas, Nucl. Phys. **A457**, 273 (1986), and references therein.
[15] A. C. Fonseca, Phys. Rev. Lett. **63**, 2036 (1989), and private communication.
[16] C. R. Howell *et al.*, Few-Body Syst. **2**, 19 (1987).
[17] G. H. Berthold, A. Stadler, and H. Zankel, Phys. Rev. Lett. **61**, 1077 (1988); Phys. Rev. C **41**, 1365 (1990).
[18] G. Bencze *et al.*, Phys. Rev. C **35**, 1188 (1987).
[19] W. Tornow, C. R. Howell, R. L. Walter, and I. Šlaus, Phys. Rev. C **45**, 459 (1992).
[20] W. Grüebler, in *Proceedings of the Symposium on Spin and Symmetries*, edited by W. D. Ramsay and W. T. H. van Oers (TRIUMF, Vancouver, Canada, 1989).
[21] B. Zeitnitz *et al.*, Nucl. Phys. **A221**, 269 (1974).
[22] G. G. Ohlsen, R. E. Brown, F. D. Correll, and R. A. Hardekopf, Nucl. Instrum. Methods **179**, 283 (1981).
[23] W. Haeberli, in *Nuclear Spectroscopy and Reactions*, edited by J. Cerny (Academic Press, New York, 1974), Pt. A, p. 151.
[24] T. Clegg, G. Bissinger, and T. Trainor, Nucl. Instrum. Methods **120**, 445 (1974).
[25] G. G. Ohlsen and P. W. Keaton, Jr., Nucl. Instrum. Methods **109**, 41 (1973); R. C. Byrd, P. W. Lisowski, W. Tornow, and R. L. Walter, Nucl. Phys. **A404**, 29 (1983).
[26] G. G. Ohlsen, Technical Report No. LA-4451, Los Alamos Scientific Laboratory of the University of California, 1970.